Spectrochimica Acta Part A: Molecular and Biomolecular Spectroscopy 263 (2021) 120142

Contents lists available at ScienceDirect

Spectrochimica Acta Part A: Molecular and Biomolecular Spectroscopy

journal homepage: www.elsevier.com/locate/saa

High-pressures study by Raman spectroscopy and DFT calculations of L-tyrosine hydrobromide crystal

C.A.A.S. Santos [a,b,e,*], R.J.C. Lima [a], W. Paraguassu [d], J.G. da Silva Filho [a], A.O. dos Santos [a], J.A. Lima Jr. [c], P.T.C. Freire [c], P.F. Façanha Filho [a]

[a] Centro de Ciências Sociais, Saúde e Tecnologia, Universidade Federal do Maranhão, Imperatriz, MA 65900-410, Brazil
[b] Centro de Ciências Humanas Sociais Tecnologias e Letras, Universidade Estadual da Região Tocantina do Maranhão, Açailândia, MA 65930-000, Brazil
[c] Departamento de Física, Universidade Federal do Ceará, Fortaleza, CE 60455-760, Brazil
[d] Instituto de Ciências Exatas e Naturais, Universidade Federal do Pará, Belém, PA 66075-110, Brazil
[e] Núcleo de Engenharias – Faculdade de Imperatriz, Imperatriz, MA 65900-120, Brazil

HIGHLIGHTS

- A Raman scattering study under high-pressures was performed in LTHBr crystals.
- DFT calculations enabled precision mode assignments.
- The molecules showed high flexibility in the lattice mode region under pressure.
- The material showed structural phase transition and conformational phase transition.

GRAPHICAL ABSTRACT

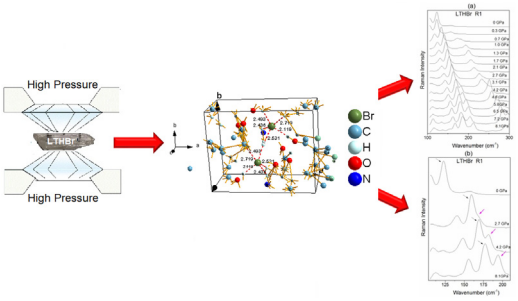

ARTICLE INFO

Article history:
Received 23 February 2021
Received in revised form 24 June 2021
Accepted 30 June 2021
Available online 06 July 2021

Keywords:
Hydrostatic pressure
Halogen ion
Raman spectroscopy
L-tyrosine hydrobromide

ABSTRACT

The high-pressure Raman spectra of L-tyrosine hydrobromide crystal (LTHBr) were obtained from 1.0 atm to 8.1 GPa in the 100–3200 cm^{-1} spectral region. The structural conformation and dimensions of the monoclinic unit cell were estimated using the powder X-ray diffraction (PXRD) method and Rietveld refinement using the GSAS program. At atmospheric pressure, the Raman spectrum was obtained in the spectral range of 100–3200 cm^{-1} and the assignment of the normal modes based on density functional theory calculations was provided. Large wavenumber shifts of modes at 106, 123, and 157 were observed, which were interpreted as the large displacement of the atoms, making the molecule a flexible structure. The change in the slope ($d\omega$ / dP) of these bands between the pressures of 3.0 and 4.0 GPa and the appearance of a mode of low wavenumber indicate the occurrence of a structural phase transition. A band initially observed at 181 cm^{-1} in the spectrum recorded at 0.7 GPa change the relative intensity with a band at 280 cm^{-1} (recorded at 5.8 GPa), indicating a conformational transition. In the region of the internal modes, the spectra show changes that reinforce the conformational phase transition since the bands initially at 1247 and 1264 cm^{-1} observed at 1.0 GPa have their intensities reversed, and at 3.0 GPa it is observed the fusion of the bands at 1264 and 1290 cm^{-1} (values recorded at ambient pressure). Thus, we can assume that the LTHBr crystal has undergone a structural phase transition and a conformational phase transition in the pressure range investigated.

1. Introduction

Currently, there is a need to improve the technological devices used by society, thus justifying the synthesis of new materials that

* Corresponding author at: Centro de Ciências Sociais, Saúde e Tecnologia, Universidade Federal do Maranhão, Imperatriz, MA 65900-410, Brazil.
E-mail address: carlos.santos@uemasul.edu.br (C.A.A.S. Santos).

https://doi.org/10.1016/j.saa.2021.120142
1386-1425/

have the purpose of meeting this need. New materials with high optical non-linearity are important due to their practical application in information technology and industrial devices [1–3]. This is due to the possibility of generating a highly efficient second harmonic, enabling the application in photonics, therefore, amino acid crystals can perform such applications because many of them have an asymmetric carbon atom and crystallize in non-centrosymmetric spatial groups [4].

Pressure is a thermodynamic variable that, like temperature, can be used as a parameter to study the energy of a system [5]. The main effect resulting from the application of hydrostatic pressure in solids, crystalline or not, is the reduction of the interatomic and intermolecular distances of the material and, consequently, its volume [6,7]. This decrease in volume implies an increase in the energy of the system. The effects of hydrostatic pressure are more pronounced for intermolecular bonds than for interatomic bonds [8].

The hydrogen-bond (H-bond) is the interaction responsible for the stability of a large number of complex biological molecular systems. Changes in the architecture of the H-bond can be induced by high hydrostatic pressures and can have an effect on system stabilization. This effect is seen in many aspects of high hydrostatic pressure in protein biochemistry [9].

The amino acids in their entirety behave like monovalent anions. Aspartic and glutamic acid, as well as tyrosine and cysteine, have the ability to form monovalent and divalent anions. This class of materials can form crystalline structures through various combinations, due to the large availability of cations [10]. Amino acid crystals are simpler models of organic molecules representative architecture of H-bond. The H-bond network is composed of an amino group and a carboxylic acid group linked by N-H···O bonds. Thus, the study of hydrogen bonds under high pressure can provide valuable information to probe the stability of the biological molecular systems. For example, L-alanine crystal is a stable molecular system [11]. On the other hand, some amino acid compounds have been investigated in the search for structural phase transition and conformational phase transition in crystals, in particular, by Raman spectroscopy techniques [12–19].

L-tyrosine hydrobromide (LTHBr) is a semi-organic non-linear optical material (NLO) and is shown to be suitable for photonic, optoelectronic device fabrication, and laser related applications [20,21]. In a previous study with L-tyrosine hydrochloride crystal (LTHCl) [22] the high-pressure Raman spectra were obtained from 1.0 atm to 7.0 GPa, indicating, that the crystal remained in the same monoclinic structure of the ambient pressure. LTHCl at a pressure of 1 atm has an intense band at 125 cm^{-1} (A1) associated with the twisting of the L-tyrosine molecule; between 0.5 and 1.0 GPa it shows a shoulder that at 3.0 GPa has an intensity inversion with the mode initially recorded at 125 cm^{-1}. In addition, this A1 mode also showed a variation in the $d\omega/dP$ slope between 1.0 and 1.5 GPa. These changes characterized a conformational phase transition undergone by the LTHCl crystal. In the external modes region, there were no major changes around 3.0 GPa and in the decompression process, it was observed that the conformational phase transition was reversible, without hysteresis. Therefore, Raman spectroscopy is a powerful experimental technique for obtaining information on changes in H bonds, studying the vibrational behavior of amino acid crystals [23]. The interpretation of Raman spectra of amino acids can provide an important contribution to the study of changes in hydrogen bonds under pressure variation and the stability of biological molecular systems [24,25].

In this research, we describe the effect of high pressure on the crystal of L-tyrosine hydrobromide (LTHBr) in the range between 1 atm and 8.2 GPa, with special attention to the bands in the spectral region of the external modes (below 200 cm^{-1}) where it is possible to collect evidence of structural and conformational phase transitions. We also show calculations using functional density theory (DFT), providing accurate assignment of the normal modes of vibration. In addition, the role of the amino acid side chain in the configuration of the hydrogen bond network and the stability of the structure are discussed.

2. Material and methods

2.1. Material synthesis

L-tyrosine hydrobromide (LTHBr) single crystals were crystalized from an aqueous solution by the slow evaporation technique using L-tyrosine (98%; Sigma-Aldrich) and hydrobromic acid (48%; Sigma-Aldrich) with stoichiometric ratio 1:1. The hydrogenic potential (pH) was measured at a value of 2.1, and temperature control was made without exceed the value of 323 K. The solution was sealed with plastic wrap which was then punched and placed in the crystal growth chamber maintained at room temperature of 298 K. The crystals were obtained typically after 3 weeks.

2.2. X-ray diffraction

The LTHBr powder sample was subjected to X-ray diffraction and data were collected with a powder diffractometer Rigaku Mini-flex II using Cu Kα (λ = 1.5418 Å) radiation. The diffraction patterns were carried out in the 2θ angular range 5–50° with a step size of 0.02° and with a counting time of 2 s/step. The structural characterization of LTHBr was obtained by Rietveld refinement using the GSAS program [26].

2.3. Raman spectroscopy and high-pressure measurements

High pressure Raman spectra were recorded in back scattering geometry using a microscope attached to a triple-grating spectrometer Jobin Yvon T64000. For Raman measurements, the 514.5 nm line of an Ar-Kr ion laser was used as excitation and the spectral resolution was set to 2 cm^{-1}. To achieve high pressures, a Diacell® μScopeDAC-RT(G) diamond anvil cell from Almax EasyLab with 0.4 mm culets diamonds was used. The sample was loaded into a 100 mm hole drilled in a stainless-steel gasket with a thickness of 200 mm using an Almax EasyLab electric discharge machine. Nujol served as the pressure transmitting medium (PTM) and the main purpose of the compressor medium is to keep the sample under hydrostatic conditions; this mineral oil is relatively hydrostatic up to 10 GPa [27–29]. The pressures were measured based on the shifts of the R1 and R2 ruby fluorescence lines.

2.4. Computational details

The structural and vibrational properties of the monoclinic structure of L-tyrosine hydrobromide crystal were investigated with the QUANTUM-ESPRESSO plane-wave code [30], which uses density functional theory [31,32]. The initial structure was based on the experimental crystallographic data reported for the L-tyrosine hydrochloride crystal [33]. For the exchange–correlation potential, the local density approximation (LDA) [34] was adopted, considering the Perdew-Zunger [35] functional with 4 × 4 × 4 MonkHorst-Pack [36] K-points and a plane waves cut off of 250 Ry. For the dispersion correction, Grimme-D2 method was used [37]. The structure was completely relaxed, including the cell parameters, until the forces became less than 1×10^{-4} Ry/Bohr, stress less than 0.01 kbar and the energy threshold set to 1×10^{-12} Ry. The relaxed lattice parameters were found to be a = 11.153 Å, b = 8.707 Å, c = 4.942 Å and β = 90.032°.

Vibrational frequencies were evaluated from the dynamical matrix calculated by the density-functional perturbation theory (DFPT), also implemented in QUANTUM-ESPRESSO [34]. Taking into account the periodic boundary conditions, this method is able to simulate vibrational spectra of different hydrogen-bonded crystals in good agreement with experimental data [38]. The dynamical matrix and frequencies of the harmonic phonon modes were coalculated using the DFPT linear response method at the Gamma (Γ) point [39,40]. The computed Raman activities are based on the Placzek's theory of the Raman effect [41,42]. The theoretical Raman intensity, which simulates the measured Raman spectrum, can be calculated according to the equation:

$$I_i^R = \frac{f(\upsilon_0 - \upsilon_i)^4 \hat{A} \cdot S_i}{\upsilon_i[1 - \exp(-hc\upsilon_i/kT)]} \quad (1)$$

where S_i is the Raman scattering activity of the ith normal mode, f is a suitable normalization factor for all peak intensities (10^{-13}). The h, k, c and T are Plank and Boltzmann constants, speed of light and temperature in Kelvin, respectively. The simulated spectra were plotted using a Lorentzian line shape with a full width at half maximum of 10 cm^{-1}.

3. Results and discussion

3.1. X-Ray diffraction

The Rietveld refinement and the recorded diffractogram at room temperature for the L-tyrosine hydrobromide powder sample is shown in Fig. 1(a). The comparison between the observed and calculated values gives R_{wp} = 13.34%, R_p = 9.48%, and S = 3.00 for the goodness of fit. The LTHBr crystal belongs to the space group $P2_1$ with two molecules per unit cell of monoclinic structure (Fig. 1(b)), with lattice parameters a = 11.323(4) Å, b = 9.086(3) Å, c = 5.167(3) Å, and β = 91.211(3)°. According to Rietveld refinement, the lattice parameters and the space group are in good agreement with the values found in literature [20,43]. In Fig. 1(c) 2x2 supercell is shown along the direction [001], where it is possible to notice the six hydrogen bonds.

3.2. DFT calculations

Before investigating the vibrational properties of LTHBr under high-pressure conditions, we first consider the structural properties obtained from our DFT calculations. The parameters of the equilibrium lattice and the cell volume are in accordance with the experimental result. Fig. 2(a), (b) and (c) shows Experimental (red line) and theoretical (blue line) Raman spectra of L-tyrosine hydrobromide in room temperature for wavenumber spectral ranges (a) 100–600, (b) 600–1800 and (c) 2860–3300 cm^{-1}.

As can be seen in Table 1, the relaxed lattice parameters a, b and c deviates from 1.4 to 4.4% of the experimental values, while the β angle showed a slight reduction of around 1.3%. As a consequence, the relaxed volume is about 0.6% smaller than the experimental one. This result is expected since the functional LDA generally overestimate interatomic forces, reducing their bond lengths and, consequently, their lattice parameters [44,45].

At this point, it is also important to compare the bond lengths and bond angles of LTHBr obtained from the calculation with the respective equilibrium parameters of correlated systems. Table 2 shows a comparison between the optimized bond lengths and bond angles computed at LDA with those reported for the monoclinic L-tyrosine hydrochloride (LTHCl) system at the same level of theory [22].

As can be seen, in general, deviations in bond length are negligible. However, a greater difference in C-O carboxylic bond lengths (~0.5%) is found between the crystals of LTHBr and LTHCl. In addition, the hydrogen bond distances on LTHBr are much greater (1.5 – 10.5%) than those found in LTHCl crystals, with the exception of β3(N-H3···Br), which is 11.32% smaller. Interestingly, a similar behavior is observed along the bond angles. The notable deviations in the angles are related to the carboxyl group C2-C1-O1 (0.55%) and hydrogen bond angles. In particular, in the LTHBr system, the bond angle associated with β3(N-H3···Br) is 132.4°, while the

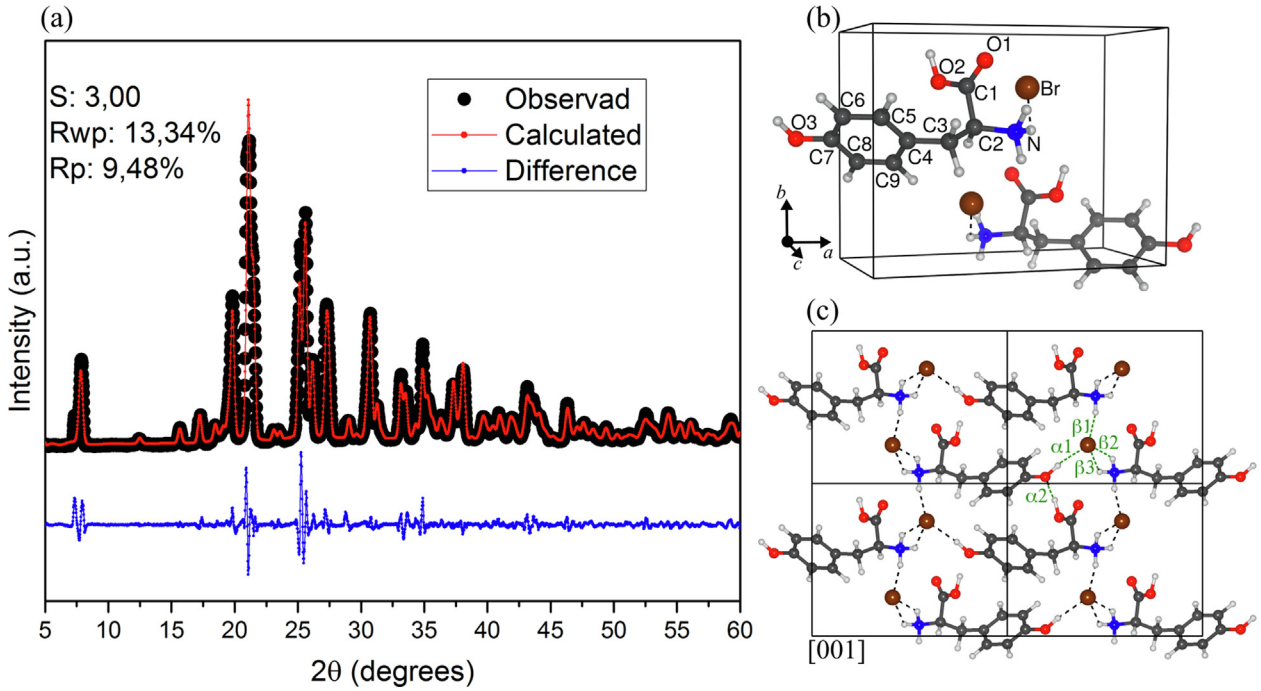

Fig. 1. (a) Rietveld refinement at room temperature of the XRD pattern of LTHBr. (b) Monoclinic unit cell of L-tyrosine hydrobromide. (c) 2x2 supercell along the [001] axis showing the six hydrogen bonds (δ1 to δ6) that holds the crystal lattice together.

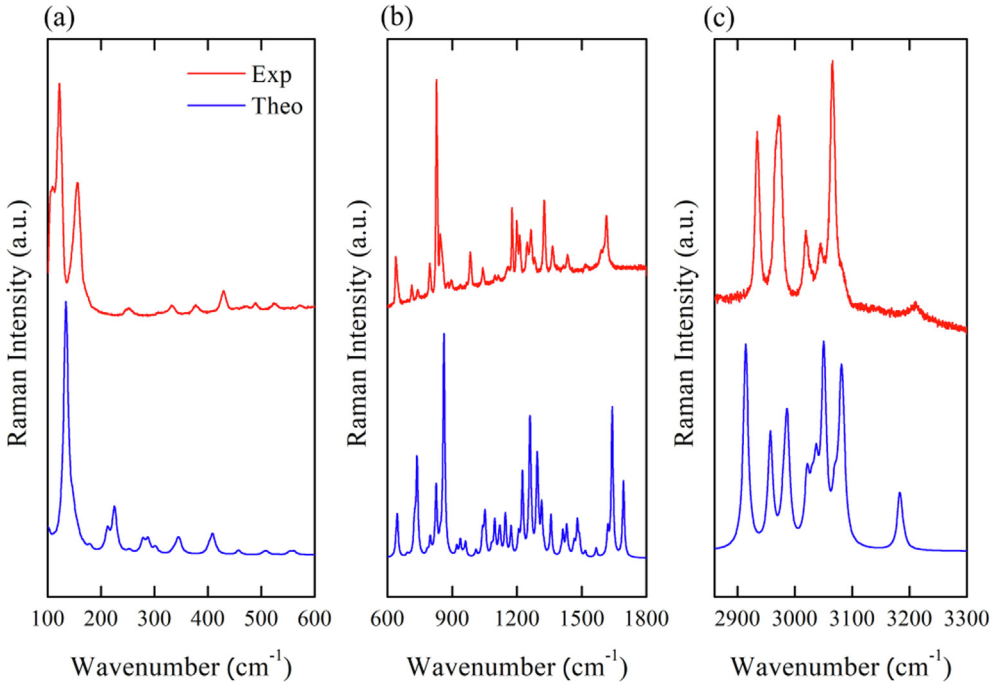

Fig. 2. Experimental (red line) and theoretical (blue line) Raman spectra of L-tyrosine hydrobromide crystal for the (a) 100–600, (b) 600–1800 and (c) 2860–3300 cm^{-1} wavenumber spectral ranges. (For interpretation of the references to colour in this figure legend, the reader is referred to the web version of this article.)

Table 1
Optimized lattice parameters of LTHBr at DFT-LDA level, compared with those obtained experimentally.

Lattice parameter	DFT-LDA	X-ray	Δ (%)
a (Å)	11.154	11.323	−1.49
b (Å)	8.708	9.086	−4.17
c (Å)	4.943	5.167	−4.34
β (°)	90.033	91.211	−1.29
V ($Å^3$)	480.064	531.466	−9.67

corresponding angle in LTHCl is much smaller, around 116.6°. It is important to note that the atomic radius of chlorine (0.97 Å) is smaller than that of bromide (1.12 Å) and, accordingly our calculations, this appears to profoundly affect the hydrogen bond interactions between tyrosine and the Br ion compared to the LTHCl system. These results indicate that particular structural and vibrational properties must be found, as will be discussed later, in the LTHBr crystals under high-pressure conditions. Table 3 shows the mode assignments for the LTHBr crystal. The attributions obtained by the theoretical spectra are in accordance with some references related to the LTHBr crystals [46].

3.3. High-pressures Raman

High pressure has been used to study properties of materials under exceptional thermodynamics conditions [47], to produce new materials [48] or to synthesize others with high purity [49]. The search for an accurate understanding of the behavior of materials under high pressure is an ongoing subject of research. In the present paper, we show high-pressure Raman spectroscopic measurements performed on the LTHBr crystal in the range of 0.0 to 8.1 GPa. The region comprising the spectral range from 100 cm^{-1} to 500 cm^{-1} was called R1. As shown in Fig. 3(a), the strongest band at 123 cm^{-1} (bending ring CC) remains until the final pressure of 8.1 GPa, different from the corresponding mode in LTHCl [22], which suffers a great loss of intensity with increasing pressure. In Fig. 3(a), we also show the decompression (back) spectrum in red. All other subsequent regions also show the decompression spectra in red. In the supplementary material, we present five figures with comparative spectra of compression (black lines) and

Table 2
The DFT/LDA calculated geometrical parameters (bond lengths in Å, angles in °) of L-tyrosine hydrobromide and L-tyrosine hydrochloride [44].

Bond lengths (Å)	LDA/LTHBr	LDA/LTHCl [40]	Δ (%)
C1-C2	1.50	1.50	0.27
C2-C3	1.52	1.52	−0.15
C3-C4	1.49	1.48	0.09
C4-C5	1.38	1.39	−0.01
C5-C6	1.38	1.38	0.03
C6-C7	1.38	1.38	−0.04
C7-C8	1.38	1.39	−0.01
C8-C9	1.38	1.38	−0.07
C1-O1	1.22	1.23	−0.50
C1-O2	1.30	1.30	0.43
C7-O3	1.36	1.36	0.03
C2-N	1.46	1.46	−0.07
α1(O3-H···Br)	2.09	1.89	10.48
α2(O2-H···O3)	1.47	1.45	1.58
β1(N-H^1···Br)	2.28	2.05	11.54
β2(N-H^2···Br)	2.37	2.20	7.84
β3(N-H^3···Br)	2.54	2.86	−11.32
Bond angle (°)			
C1-C2-C3	109.1	108.4	0.64
C2-C3-C4	113.5	115.4	−1.64
C3-C4-C5	120.7	120.1	0.47
C4-C5-C6	121.4	121.5	−0.07
C5-C6-C7	119.3	119.3	−0.01
C6-C7-C8	120.4	120.3	0.05
C7-C8-C9	119.5	119.6	−0.05
C2-C1-O1	121.7	121.0	0.55
O1-C1-O2	126.2	126.2	0.02
C6-C7-O3	122.1	121.7	0.35
C1-C2-N	108.8	109.6	−0.77
α1(O3-H···Br)	164.0	168.3	−2.55
α2(O2-H···O3)	171.5	172.0	−0.28
β1(N-H^1···Br)	167.5	165.3	1.32
β2(N-H^2···Br)	143.0	143.9	−0.64
β3(N-H^3···Br)	132.4	116.5	13.72

Table 3
Selected mode analysis: Observed Raman band positions (ω_{exp}), calculated vibrational wavenumbers (ω_{cal}), assignments for L-tyrosine hydrobromide crystal.

ω_{exp} (cm^{-1})	ω_{cal} (cm^{-1})[a]	sym[c]	Assignments[b]	ω_{exp} (cm^{-1})	ω_{cal} (cm^{-1})[a]	sym[c]	Assignments[b]
106	111	B	t(O3···HO2C1O1)	1041	1097	B	ν(C2N) + δ(C3H2) + δ_{ring}(CH)
123	134	A	δ_{ring}(CC)	1154	1207	A	ν(C3C4) + δ(C3H2) + δ_{ring}(CH) + δ(O3H) + δ(O2H)
157	225	A	ρ(NH3)	1178	1225	A	δ(C2H) + δ(C3H2) + δ_{ring}(CH) + δ(O3H) + δ(O2H)
248	278	A	τ(NC2C1O2)	1200	1260	A	δ_{ring}(CH) + ν(C7O3) + ν(C1O2)
333	347	A	φ(NC2C3C4) + δ(NH3)	1213	1265	A	δ(C2H) + δ(C3H2) + ν(C7O3) + ν(C1O2)
378	409	A	τ_{ring}(CC) + τ(NC2C3C4) + ρ(NH3)	1247	1293	A	δ_{ring}(CH) + δ(O3H) + δ(O2H)
430	458	B	tw_{ring}(CC) + ν(O3···HO2)	1264	1314	A	δ_{ring}(CH) + δ(O3H) + δ(O2H)
488	510	B	wag_{ring}(CC) + ν(O3···HO2)	1326	1357	B	wag(C3H) + wag(NH3) + δ(O3H) + δ(O2H)
525	553	A	wag_{ring}(CH) + ν(O3···HO2)	1364	1412	A	ν_{ring}(CC) + sc(C3H)
640	645	A	ρ($C3H_2$) + δ(O3H) + τ(O1-C1-C2-C3)	1434	1479	B	sc(NH_3)
713	736	A	wag_{ring}(CC)	1588	1621	A	ν_{ring}(CC)
742	797	A	wag_{ring}(CH)	1616	1694	B	sc(NH2) + ν(O1C1)
797	825	A	wag_{ring}(CH)	2934	2914	A	νs(C3H2) + ν(C2H)
828	861	A	wag_{ring}(CC) + sc(O1C2O2)	2971	2957	B	νa(C3H2) + ν(C2H)
848	863	B	wag_{ring}(CC) + sc(O1C2O2)	3020	2987	B	ν(O2H) + ν(O3H) + νa(NH)
879	921	B	wag_{ring}(CC) + ρ(C3H2) + ρ(NH_2)	3043	3037	B	ν(O3H) + ν(C9H)
894	937	A	wag_{ring}(CC) + ρ(C3H2) + ρ(NH_2)	3066	3050	A	ν(O3H) + νs(NH3)
982	1052	B	δ(C2H) + tw(C3H2) + δ(O3H) + δ(O2H)	3209	3183	A	ν(NH)

[a] Calculated with DFT-LDA approach.
[b] Nomenclature: τ = torsion; δ = bending; sc = scissoring; tw = twisting; φ = out-of-plane; wag = wagging; ν = stretching; ρ = rocking; ν_{as} = asymmetric stretching; ν_s = symmetric stretching.
[c] Vibrational modes belonging to the A and B irreducible representations are non-degenerated.

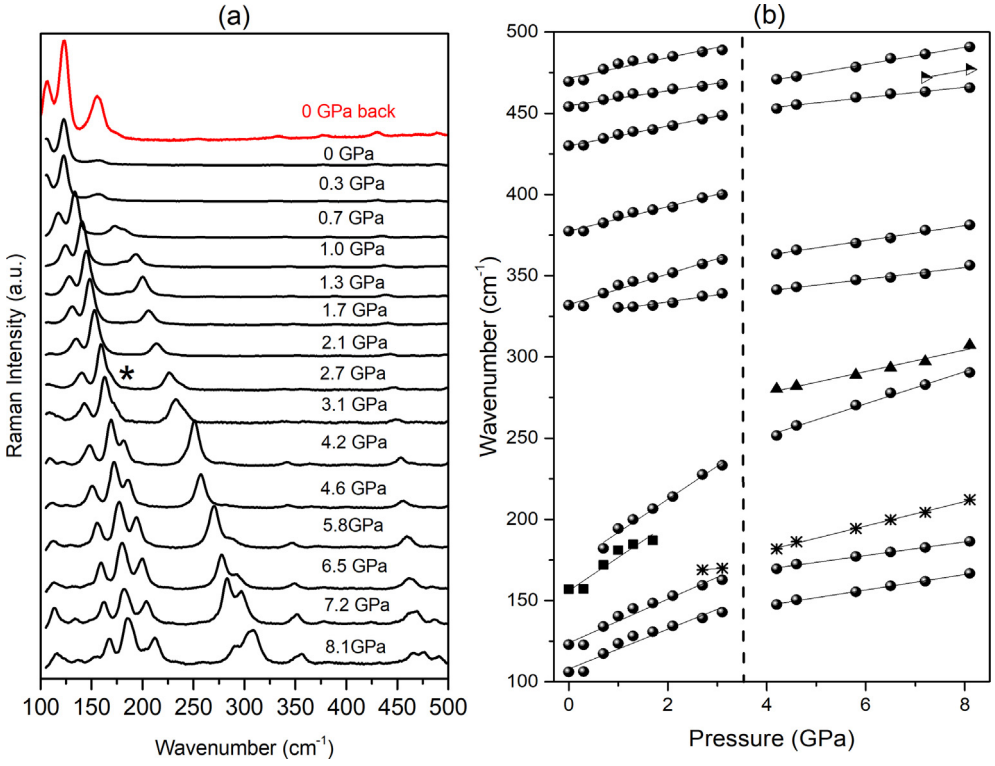

Fig. 3. (a) Raman spectra of LTHBr crystal under pressures for spectral region: 100–500 cm^{-1} and (b) Wavenumber vs. pressure plots of LTHBr for spectral region: 100–500 cm^{-1}.

decompression (red lines) for all spectral regions (R1, R2, R3, R4, and R5). At 2.7 GPa, a band appears at approximately 169 cm^{-1}; this band is indicated by an asterisk in Fig. 3(a) and 3(b). As the pressure increases, it gains considerable intensity when compared to most others in that region. The weak mode at 157 cm^{-1} (rocking NH_3), whose wavenumbers are indicated by squares in Fig. 3(b), decreases in intensity until it disappears at 2.0 GPa. But before that, another mode appears at 181 cm^{-1} when a pressure of 0.7 GPa is reached, and at 1.0 GPa these two modes undergo an inversion in their relative intensities. At 4.2 GPa, the same mode that appeared at 0.7 (181 cm^{-1}) gains even more intensity and becomes narrower and then a shoulder appears around 280 cm^{-1} (at 5.8 GPa), whose numbers of waveforms are indicated by triangles in Fig. 3(b). These two modes invert their intensities by 8.1 GPa. In addition, the high values of the dω/dP slopes (12.2, 13.5, 14.5 and 20.3 cm^{-1} / GPa) of the modes at 106, 123, 157 and 182 cm^{-1}, respectively, demonstrate high sensitivity of these modes to the increase in pressure. Another important point to be highlighted is the change in the slope of these bands between pressures of 3.0 and 4.0 GPa. This type of behavior is currently associated with phase transitions. All of these results are shown in Fig. 3(b) and Table 4; this table shows the values for ω_{exp}, $\omega_{o,}$ and α for the linear fitting $\omega = \omega_o + \alpha P$

Table 4
Values for ω_{exp}, ω_o and α for the linear fitting $\omega = \omega_o + \alpha P$ of the LTHBr crystal in different ranges of pressure and for entire all regions.

$\omega_{exp.}$ (cm^{-1})	ω_0 (cm^{-1})	α (cm^{-1}/GPa)	Presssure range (GPa)
106	108	12.2	0.0–3.0
148	127	4.8	4.0–8.1
123	124	13.5	0.0–3.0
170	152	4.2	4.0–8.1
157	160	14.5	0.0–2.1
181	199	−1.14	4.0–8.1
169	162	2.35	2.7–3.0
198	150	7.5	4.0–8.1
182	172	20.3	0.7–3.0
251	211	9.9	4.0–8.1
280	251	6.6	4.0–8.1
248	244	6.0	0.0–8.1
332	336	6.3	0.0–8.1
378	381	6.4	0.0–8.1
430	433	4.5	0.0–8.1
454	457	4.6	0.0–8.1
470	476	5.1	0.0–8.1
489	494	3.6	0.0–8.1
525	531	4.6	0.0–8.1
640	641	0.8	0.0–8.1
655	652	2.6	1.0–8.1
713	716	2.4	0.0–8.1
741	744	1.3	0.0–8.1
773	773	0.8	0.0–8.1
797	798	2.8	0.0–8.1
830	831	3.7	0.0–8.1
847	848	5.7	0.0–8.1
862	862	5.9	0.7–8.1
897	898	3.3	0.0–8.1
983	986	3.2	0.0–8.1
982	986	3.2	0.0–8.1
1041	1049	4.1	0.0–8.1
1071	1080	5.3	0.0–8.1
1155	1148	1.8	0.0–8.1
1178	1180	1.9	0.0–8.1
1200	1202	1.8	0.0–8.1
1213	1214	2.9	0.0–8.1
1247	1251	4.2	0.0–8.1
1265	1269	3.6	0.0–8.1
1290	1292	0.5	0.0–8.1
1417	1416	−0.52	0.7–8.1
1441	1440	3.2	0.0–8.1
1458	1458	4.3	0.0–8.1
1523	1522	2.6	0.7–8.1
1586	1585	1.7	0.0–8.1
1613	1608	2.8	2.1–8.1
1616	1613	2.1	0.0–8.1
2855	2853	12.8	0.0–3.1
2902	2901	−1.83	4.2–8.1
2934	2935	6.2	0.0–3.1
2953	2941	3.9	4.2–8.1
2965	2971	5.0	0.0–8.1
3021	3022	5.7	0.0–8.1
3066	3068	6.3	0.0–8.1

of the LTHBr crystal in different pressure ranges and for all spectral regions.

It would be instructive to compare the behavior of Raman spectra of L-tyrosine hydrobromide and L-tyrosine hydrochloride crystals under pressure. We highlight the following points: a) for the LTHBr crystal, while the strongest band remains up to 8.1 GPa (still as the strongest band), for the LTHCl crystal the corresponding band lost intensity rapidly and by 3.5 GPa this band already has very low intensity. b) Change of slope dω/dP for LTHBr between 3.0 and 4.0 GPa, while for LTHCl it occurs between 1.0 and 1.5 GPa. c) While new bands are observed for LTHBr (P > 3.1 GPa), no new bands were observed for LTHCl even across the entire pressure range. Based on the above characteristics of both crystals, we propose a structural phase transition undergone by LTHBr crystal from 3.1 to 4.2 GPa and a conformational transition from 5.8 GPa to 8.1 GPa. In view of the structural similarity of these two crystals, the alteration of the halides seems to play an important role in the behavior of the pressure-induced phase transitions for these types of crystals.

The region of the spectral range from 560 cm^{-1} to 960 cm^{-1} was called R2. Fig. 4(a) presents the Raman spectra of LTHBr crystal in the pressure range of 0.0 to 8.1 GPa and a spectral range of 560–960 cm^{-1}. Fig. 4(b) shows the behavior of the wavenumber as a function of pressure for the range 600 to 960 cm^{-1}.

The R2 region presents bands associated with combination of vibrations at 640 cm^{-1} (rocking $C3H_2$ + bending O3H + torsion O1-C1-C2-C3) and for wagging ring CC at 713 cm^{-1}. In addition, bands are observed at 742 cm^{-1} (wagging of ring CH), at 797 cm^{-1} (wagging of ring CH), at 828 cm^{-1} (CC wagging + scissor ing O1C2O2) the mode most intense of region, at 848 cm^{-1} (CC wagging + scissoring O1C2O2). Other bands are observed at 879 cm^{-1} (wagging of ring CC + rocking C3H2 + rocking NH_2) and 894 cm^{-1} (wagging of ring CC + rocking C3H2 + rocking NH_2). The bands for this spectral region showed low dω/dP values when compared to the bands in the wavenumber modes of R1 region. There are no considerable changes associated with this spectral range. Therefore, few changes related to the modes, except the intensity gains of the strongest band with the increase of the pressure. On the other hand, the equivalent band in the LTHCl crystal showed a loss of intensity with increasing pressure [22]. In addition, the spectra showed no significant changes with increasing pressure.

Fig. 5(a) and 5(b) show the R3 region in the pressure range from 1 atm to 8.1 GPa and a spectral range from 960 to 1300 cm^{-1} and the behavior of the wavenumber as a function of pressure for the range of 950 to 1300 cm^{-1}, respectively.

This region presents bands associated with the modes at 982 cm^{-1} (bending C2N + twisting $C3H_2$ + bending O3H + bending O2H), 1041 cm^{-1} (stretching C2N + bending $C3H_2$ + bending of ring CH), 1154 cm^{-1} (stretching C3C4 + bending $C3H_2$ + bending of ring CH + bending O3H + bending O2H), and also an intense band at 1178 cm^{-1} (bending C2H + bending $C3H_2$ + bending of ring CH + bending O3H + bending O2H) which decreases its intensity with increased pressure. The band at 1213 cm^{-1} [1] (bending C2H + bending $C3H_2$ + stretching C7O3 + stretching C1O2) at ambient pressure decreases in intensity until it almost disappears at 8.1 GPa pressure. The two neighboring modes at 1247 (bending of ring CH + bending O3H + bending O2H), 1265 cm^{-1} (bending of ring CH + bending O3H + bending O2H), exhibit behavior that reinforces the evidence of conformational phase transition, since these bands at 1.0 GPa inverts their intensities. The band at 1247 cm^{-1} has a weak intensity in the spectrum at 1 atm, while this same mode becomes the strongest at 8.1 GPa. In addition to this band gaining intensity, it undergoes significant shifts with increased pressure when compared to the neighboring band with the highest wavenumber. From Table 3, the band at 1247 cm^{-1} is associated with bending of ring CH + bending O3H + bending O2H and, therefore, participates in the hydrogen bond network. Therefore, changing the hydrogen bond configuration can trigger anomalies related to this band.

Fig. 6(a) and 6(b) show the R4 region in the pressure range from 1 atm to 8.1 GPa and the spectral range 1400–1800 cm^{-1} and the behavior of the wavenumber as a function of pressure for the spectral range from 1400 to 1660 cm^{-1}, respectively.

This region presents band associated with the 1434 cm^{-1} (NH_3 scissoring). These two neighboring bands form the largest band in this region. The weak band at 1588 cm^{-1} (CC stretching of ring) and the band at 1616 cm^{-1} (NH_2 scissoring + O1C1 stretching) both initially at ambient pressure, visually invert their intensities to P > 2.7 GPa. Therefore, these doublets evidenced different Raman behavior associated with a unit connected to the hydrogen bond network and another associated with the imidazole ring. On the

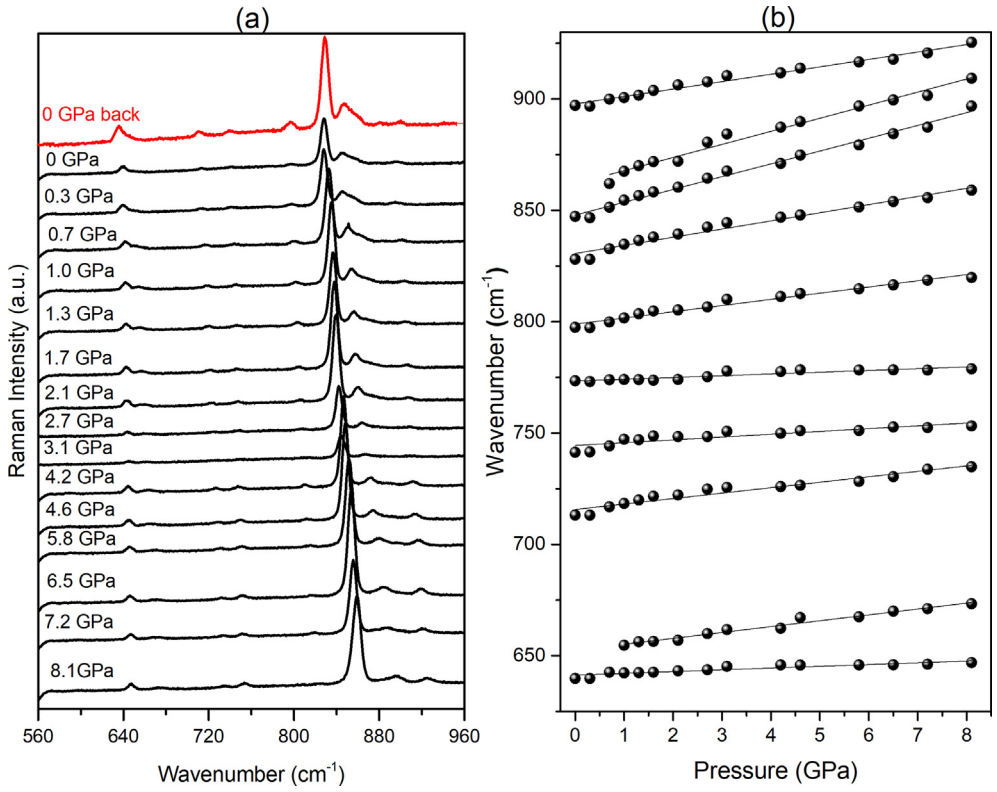

Fig. 4. (a) Raman spectra of LTHBr crystal under pressures for spectral region: 560–960 cm^{-1} and (b) Wavenumber vs. pressure plots of LTHBr for spectral region: 600–960 cm^{-1}.

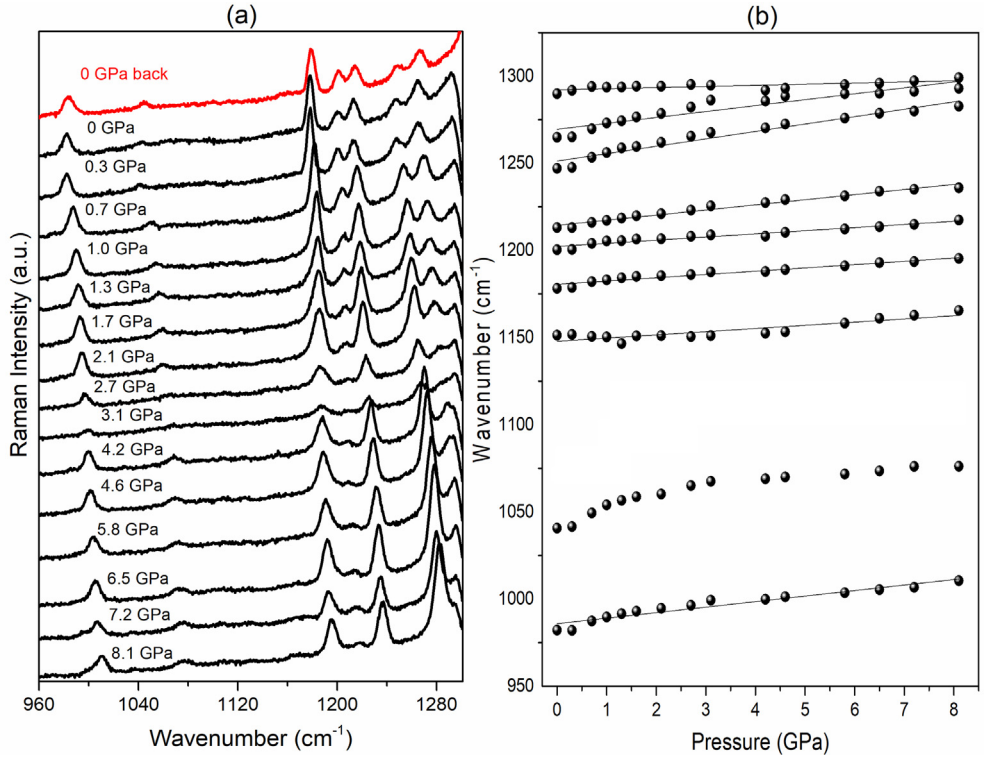

Fig. 5. (a) Raman spectra of LTHBr crystal under pressures for spectral region: 960–1300 cm^{-1} and (b) Wavenumber vs. pressure plots of LTHBr for spectral region: 950–1350 cm^{-1}.

other hand, the LTHCl crystal did not show an inversion of intensities in relation to these bands under pressure. In fact, the corresponding band around 1588 cm^{-1} loses intensity up to 7.2 GPa [22]. This behavior demonstrates the role of halides in linking the lattice modes to the internal modes involved in hydrogen bonds.

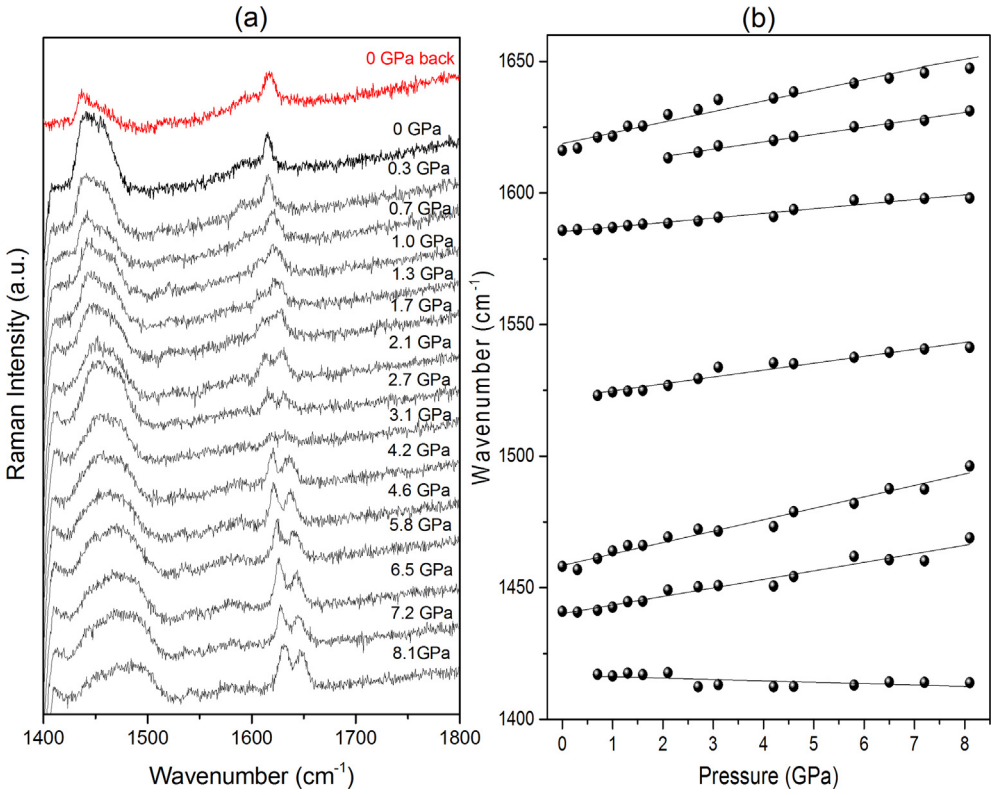

Fig. 6. (a) Raman spectra of LTHBr crystal under pressures for spectral region: 1400–1800 cm^{-1} and (b) Wavenumber vs. pressure plots of LTHBr for spectral region: 1400–1660 cm^{-1}.

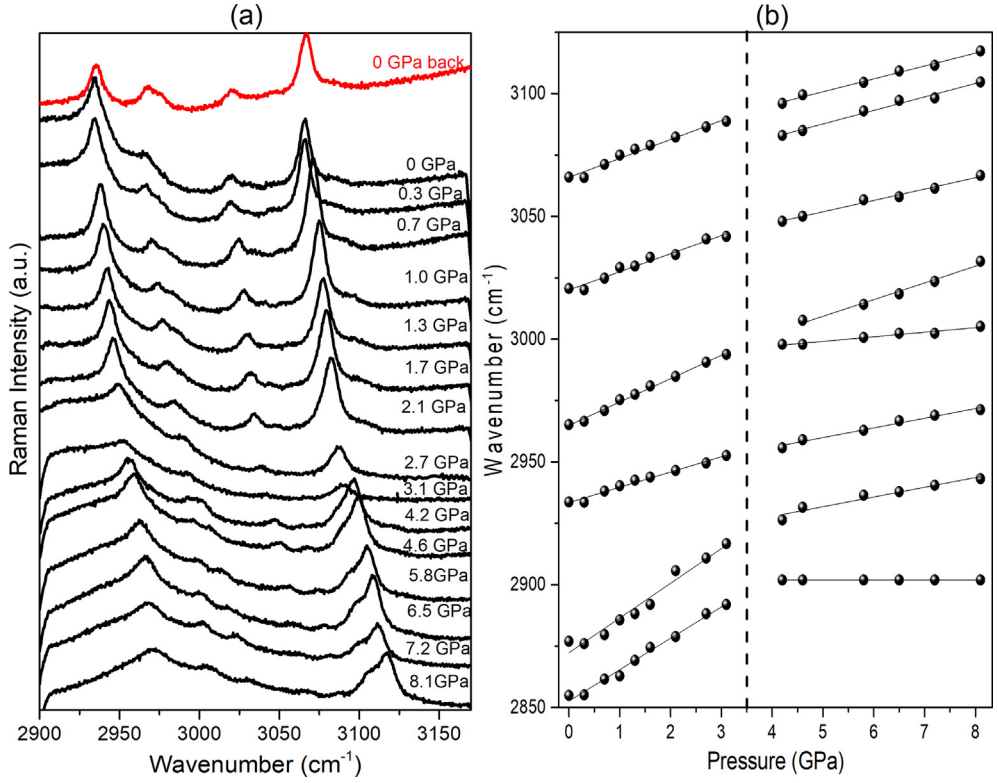

Fig. 7. (a) Raman spectra of LTHBr crystal under pressures for spectral region: 2900–3170 cm^{-1} and (b) Wavenumber vs. pressure plots of LTHBr for spectral region: 2850–3125 cm^{-1}.

The R5 region shows the high energy Raman spectra in the spectral range between 2900 cm^{-1} and 3170 cm^{-1} for the LTHBr crystal. Fig. 7(a) and 7(b) show this region in the pressure range of 1 atm to 8.1 GPa and the behavior of the wavenumber as a function of pressure in the range of 2850–3125 cm^{-1}.

R5 region is characterized by the presence of axial deformations (symmetric and anti-symmetric stretching). These vibrational modes correspond to the bands at 2934 cm^{-1} ($C3H_2$ symmetric stretching and stretching C2H) and 2971 cm^{-1} (C2H stretching and $C3H_2$ anti-symmetric stretching). At ambient pressure, the bands can be seen at 3020 cm^{-1} (NH anti-symmetric stretching + O2H stretching + O3H stretching) and 3066 cm^{-1} (NH_3 symmetric stretching + stretching O3H). Two new bands appear, initially as shoulders, the first at about 3085 cm^{-1} at 4.2 GPa and a weak band at 3007 cm^{-1}, at 4.5 GPa. All bands in this region shift to higher wavenumbers (blue shift) losing definition and intensity, a fact possibly related to the conformational disorder induced by the increasing pressure.

At ambient pressure, the complexed structure of L-tyrosine (LT), LTHBr and LTHCl, are structurally similar, both are monoclinic, have two molecules per unit cell, and present the same spatial group $P2_1$ [20,22,33,46]. Both LTHBr and LTHCl have their molecules interconnected by O - H ··· O and N - H ···X bonds (X = Br, Cl). As noted earlier, the temperature decomposition process is dominated by the N-H…X bonds, with little contribution from the O-H…O bonds [43]. The insertion of Br^- and Cl^- ions in the LT structure confers some similarity between the vibrational properties of the LTHBr and LTHCl crystals [22,43]. For LTHCl, almost no change in the spectral region associated with the internal modes was observed under high pressure; only a highly intense bond with low wavenumber undergoes noticeable change [22]. On the other hand, in our present high-pressure study of LTHBr, we were able to observe changes both in the internal modes region and in the lattice modes region. Thus, although there is some similarity in the vibrational properties, the pressure evolution is diverse, as well as the pressure ranges where the two structures are stable: the original phase is observed up to 1.5 GPa for LTHCl and up to ~ 3.0 GPa for LTHBr. Interestingly, the H – Cl distances vary from 2.378 to 2.505 Å in the N - H···Cl bonds for LTHCl, while the H – Br distances vary from 2.436 to 2.531 Å in the N - H ··· Br bonds for LTHBr. Apparently, the longer H bonds makes the structure a little more flexible, allowing the crystal to maintain its symmetry without the need to change its monoclinic structure. Comparing the compression and decompression spectra in all spectral regions of the LTHBr crystal, we note that there is similarity between them, showing that the changes are reversible, which was also observed in the LTHCl crystal [22]. Testing this hypothesis for stability of complexed structure of amino acid is important to support future applications focused on the halogen ion – organic interactions.

4. Conclusions

Raman spectroscopy measurements were performed as a function of pressure (from 1 atm to 8.1 GPa) in the LTHBr crystal in five different spectral regions: R1 (100–500 cm^{-1}), R2 (560–960 cm^{-1}), R3 (960–1300 cm^{-1}), R4 (1400–1800 cm^{-1}), and R5 (2900–3170 cm^{-1}). Mode assignments showed good agreement with the experimental spectra and were based on DFT calculations. At 2.7 GPa, a band appears at 169 cm^{-1} and with the increase in pressure it gained considerable intensity when compared to most of the others in that region of the lattice modes. The high flexibility of the L-tyrosine molecules is shown with the large displacement for larger wavenumbers of the modes in 106, 123, 157, and 182 cm^{-1}. In addition, the change in the slope ($d\omega/dP$) of these bands between pressures of 3.0 and 4.0 GPa reinforce the occurrence of a structural phase transition. The appearance of a shoulder at 5.8 GPa (280 cm^{-1}) and the inversion of subsequent pressures, points to a conformational transition that extends to 8.1 GPa. The spectra in the region of the internal modes show changes that reinforce the conformational phase transition, since the bands initially at 1247 and 1264 cm^{-1} at 1.0 GPa invert their intensities, and at 3.0 GPa the merger of the modes recorded at 1264 and 1290 cm^{-1} at ambient pressure. The decompression spectra are similar to the spectra before compression, so this similarity reinforces those spectral changes observed throughout the compression run are in fact reversible. Thus, we can assume that the LTHBr crystal possibly underwent a conformational phase transition accompanied by a structural phase transition.

CRediT authorship contribution statement

C.A.A.S. Santos: Investigation, Writing - review & editing. **R.J.C. Lima:** Investigation. **W. Paraguassu:** Investigation. **J.G. Silva Filho:** Investigation. **A.O. Santos:** Investigation. **J.A. Lima:** Writing - Review & Editing. **P.T.C. Freire:** Writing - review & editing. **P.F. Façanha Filho:** Writing - review & editing, Project administration.

Declaration of Competing Interest

The authors declare that they have no known competing financial interests or personal relationships that could have appeared to influence the work reported in this paper.

Acknowledgements

The authors thank FAPEMA and CNPq for financial support and Electronic and Vibrational Spectroscopy Group (GEEV) - Department of Physics of Federal University od Pará (UFPA) for support from the high-pressure measurements.

Appendix A. Supplementary data

Supplementary data to this article can be found online at https://doi.org/10.1016/j.saa.2021.120142.

References

[1] R.A. Soares, R.J.C. Lima, P.F.F. Filho, P.T.C. Freire, J.A. Lima, J.G.S. Filho, High-pressure Raman study of mono-l-alaninium nitrate crystals, Phys. B Condens. Matter. 521 (2017) 317–322, https://doi.org/10.1016/j.physb.2017.07.007.
[2] T. Kar, Amino acids-precursors for synthesizing nonlinear optical materials, P. Cryst. Growth Charac. Mat. 58 (2–3) (2012) 74–83, https://doi.org/10.1016/j.pcrysgrow.2012.03.002.
[3] A.L.O. Cavaignac, R.A. Soares, R.J.C. Lima, P.F.F. Filho, P.T.C. Freire, The Behavior of the Deformation Vibration of NH3 in Semi-Organic Crystals under High Pressure Studied by Raman Spectroscopy, Crystals 8 (6) (2018) 245, https://doi.org/10.3390/cryst8060245.
[4] J.O. Carvalho, G.M. Moura, A.O. Dos Santos, R.J.C. Lima, P.T.C. Freire, P.F.F. Filho, High pressure Raman spectra of monoglycine nitrate single crystal, Spect. Acta Part A: Mol. Biom. Spect. 161 (2016) 109–114, https://doi.org/10.1016/j.saa.2016.02.031.
[5] B.A. Zakharov, E.V. Boldyreva, High pressure: a complementary tool for probing solid-state processes, Cryst. Eng. Comm. 21 (1) (2019) 10–22, https://doi.org/10.1039/C8CE01391H.
[6] F.J. Manjón, D. Errandonea, Pressure-induced structural phase transitions in materials and earth sciences, Phys. Stat. Solidi. (b) 246 (1) (2009) 9–31, https://doi.org/10.1002/pssb.200844238.
[7] J.V. Badding, High-pressure synthesis, characterization, and tuning of solid state materials, Annu. Rev. Mater. Res. 28 (1) (1998) 631–658, https://doi.org/10.1146/annurev.matsci.28.1.631.
[8] P.T.C. Freire, J.A.L. Júnior, B.T.O. Abagaro, G.S. Pinheiro, J.D.A.F. Silva, J.M. Filho, A. F.EMelo, High Pressure Raman Spectra of Amino Acid Crystals, Vib. Spect. Rijeka: InTech (2012) 37–58, https://doi.org/10.5772/32533.
[9] C. Balny, P. Masson, K. Heremans (Eds.), Frontiers in high pressure biochemistry and biophysics, Elsevier, 2002.
[10] M. Fleck, A.M. Petrosyan, Salts of Amino Acids, Springer International Publishing, Cham (2014), https://doi.org/10.1007/978-3-319-06299-0.

[11] N.P. Funnell, A. Dawson, D. Francis, A.R. Lennie, W.G. Marshall, S.A. Moggach, J. E. Warrenc, S. Parsons, The effect of pressure on the crystal structure of L-alanine, CrystEngComm 12 (2010) 2573–2583, https://doi.org/10.1039/C001296C.
[12] A. Eşme, S.G. Sağdınç, Conformational, spectroscopic (FT-IR, FT-Raman, and UV-Vis), and molecular docking studies of N-(2-hydroxyethyl) succinimide, J. Mol. Struct. 1195 (2019) 451–461, https://doi.org/10.1016/j.molstruc.2019.06.019.
[13] Y. Ren, H. Zhang, J. Zhang, X. Cheng, L. Jiang, Z. Chen, H. Dai, High-pressure induced conformational and phase transformations of 1, 4-dioxane probed by Raman spectroscopy, J. Mol. Struct. 1210 (2020), https://doi.org/10.1016/j.molstruc.2020.127987 127987.
[14] C. Luz-lima, J.A. Borges, J.V.B. Moura, G.S. Pinheiro, B.C. Viana, J. Mendes-Filho, Vibrational Spectroscopy α - L -glutamic acid under high pressure: Phase transitions studied by Raman spectroscopy, Vib. Spectrosc. 86 (2016) 343–349, https://doi.org/10.1016/j.vibspec.2016.08.012.
[15] T.L. Prazyan, Y.N. Zhuravlev, O.V. Golovko, O.S. Obolonskaya, DFT-study of pressure-induced phase transition in L-threonine, J. Mol. Struct. 1196 (2019) 271–279, https://doi.org/10.1016/j.molstruc.2019.06.077.
[16] J.S. Junior, G.D.S. Souza, C.L. Lima, P.T.C. Freire, G.S. Pinheiro, Vibrational properties of L-cysteine hydrochloride monohydrate crystal under high-pressure, Vib. Spectrosc. 98 (2018) 92–97, https://doi.org/10.1016/j.vibspec.2018.07.003.
[17] F.M.S. Victor, F.S.C. Rêgo, F.M. de Paiva, A.O. dos Santos, A. Polian, P.T.C. Freire, J.A.L. Júnior, P.F.F. Filho, Pressure-induced phase transitions in DL-glutamic acid monohydrate crystal, Spectrochim. Acta A Mol. Biomol. Spectrosc. 230 (2020), https://doi.org/10.1016/j.saa.2020.118059 118059.
[18] K.C. Gordon, C.J. McAdam, S.C. Moratti, G.E. Shillito, J. Simpson, Conformational aspects of dibenzo-tetroxecin: A structural, Raman spectroscopic and computational study, J. Mol. Struct. 1145 (3) (2017) 21–328, https://doi.org/10.1016/j.molstruc.2017.05.103.
[19] B.A. Kolesov, M.A. Mikhailenko, E.V. Boldyreva, Dynamics of the intermolecular hydrogen bonds in the polymorphs of paracetamol in relation to crystal packing and conformational transitions: a variable-temperature polarized Raman spectroscopy study, PCCP 13 (31) (2011) 14243–14253.
[20] B.N. Moolya, S.M. Dharmaprakash, Synthesis, growth and characterization of nonlinear optical crystal: L-tyrosine hydrobromide, J. Cryst. Growth 290 (2) (2006) 498–503, https://doi.org/10.1016/j.jcrysgro.2006.01.061.
[21] M. Kumari, N. Vijayan, E. Sharma, D. Nayak, S. Yadav, S. Das, R.P. Pant, Synthesis and growth of l-tyrosine hydrobromide and its characterization for optoelectronic applications, J. Mater. Sci.: Mater. Electron. 31 (21) (2020) 18524–18532, https://doi.org/10.1007/s10854-020-04396-2.
[22] C.A.A.S.S. dos Santos, J.O. Carvalho, J.G. da Silva Filho, J.L. Rodrigues, G.S. R.J.C. LimaPinheiro, P.T.C. Freire, P.F. Façanha Filho, High-pressure Raman spectra and DFT calculations of L-tyrosine hydrochloride crystal, Phys. B Condens. Matter. 531 (2018) 35–44, https://doi.org/10.1016/j.physb.2017.11.090.
[23] S.A. Siddiqui, A.K. Pandey, A. Dwivedi, S. Jain, N. Misra, Comparative conformational, structural and vibrational study on the molecular structure of tyrosine and L-DOPA using density functional theory, J. Chem. Pharm. Res 2 (4) (2010) 835–850.
[24] P.F.F. Filho, P.T.C. Freire, F.E.A. Melo, V. Lemos, J. Mendes-Filho, P.S. Pizani, D.Z. Rossatto, Pressure-induced phase transitions in L-leucine crystal, J. Raman Spectrosc. 40 (2009) 46–51, https://doi.org/10.1002/jrs.2071.
[25] J. Li, S. Lee, D. Pinnick, A. Anderson, W. Smith, R.ey Gri, V. Mohan, Raman and infrared studies of nucleosides at high pressures: II. cytidine, J. Biomol. Struct. Dynam. 19 (2002) 1111, https://doi.org/10.1080/07391102.2002.10506814.
[26] A.C. Larson, R.B. Von Dreele, General Structure Analysis System (GSAS), The Regents of the University of California, Los Alamos National Laboratory Report LAUR, Los Alamos, 2004.
[27] S. Klotz, J.C. Chervin, P. Munsch, G. Le Marchand, Hydrostatic limits of 11 pressure transmitting media, J. Phys. D Appl. Phys. 42 (2009), https://doi.org/10.1088/0022-3727/42/7/075413 075413.
[28] J.W. Otto, J.K. Vassiliou, G. Frommeyer, Nonhydrostatic compression of elastically anisotropic polycrystals. I. Hydrostatic limits of 4: 1 methanol-ethanol and paraffin oil, Phys. Rev. B. 57 (1998) 3253.
[29] M. Mączka, M. Ptak, K.P. da Silva, P.T.C. Freire, J. Hanuza, High-pressure Raman scattering and an anharmonicity study of multiferroic wolframite-type Mn0.97Fe0.03WO4, J. Phys. Condens. Matter 24345403 (34) (2012), https://doi.org/10.1088/0953-8984/24/34/345403.
[30] P. Giannozzi, S. Baroni, N. Bonini, M. Calandra, R. Car, C. Cavazzoni, D. Ceresoli, G.L. Chiarotti, M. Cococcioni, I. Dabo, A. Dal Corso, S. de Gironcoli, S. Fabris, G. Fratesi, R. Gebauer, U. Gerstmann, C. Gougoussis, A. Kokalj, M. Lazzeri, L. Martin-Samos, N. Marzari, F. Mauri, R. Mazzarello, S. Paolini, A. Pasquarello, L. Paulatto, C. Sbraccia, S. Scandolo, G. Sclauzero, A.P. Seitsonen, A. Smogunov, P. R.M. Umari, QUANTUM ESPRESSO a modular and open-source software project for quantum simulations of materials, J. Phys. Condens. Matter. 21395502 (2009), https://doi.org/10.1088/0953-8984/21/39/395502.
[31] P. Hohenberg, W. Kohn, Inhomogeneous Electron Gas, Phys. Rev. B. 136 (1964) B864, https://doi.org/10.1103/PhysRev.136.B864.
[32] W. Kohn, L.J. Sham, Self-Consistent Equations Including Exchange and Correlation Effects, Phys. Rev. 140 (1965) A1133–A1138, https://doi.org/10.1103/PhysRev.140.A1133.
[33] M.N. Frey, T.F. Koetzle, M.S. Lehmann, W.C. Hamilton, Precision neutron diffraction structure determination of protein and nucleic acid components. X. A comparison between the crystal and molecular structures of L-tyrosine and L-tyrosine hydrochloride, J. Chem. Phys. 58 (1973) 2547–2556, https://doi.org/10.1063/1.1679537.
[34] S. Baroni, S. De Gironcoli, A. Dal Corso, P. Giannozzi, Phonons and related crystal properties from density-functional perturbation theory, Rev. Mod. Phys. 73 (2001) 515–562, https://doi.org/10.1103/RevModPhys.73.515.
[35] J.P. Perdew, A. Zunger, Self-interaction correction to density-functional approximations for many-electron systems, Phys. Rev. B. 23 (1981) 5048–5079, https://doi.org/10.1103/PhysRevB.23.5048.
[36] H.J. Monkhorst, J.D. Pack, Special points for Brillouin-zone integrations, Phys. Rev. B. 13 (1976) 5188–5192, https://doi.org/10.1103/PhysRevB.13.5188.
[37] S. Grimme, Semiempirical GGA-type density functional constructed with a long-range dispersion correction, J. Comput. Chem. 27 (2006) 1787–1799, https://doi.org/10.1002/jcc.20495.
[38] K. Lejaeghere, G. Bihlmayer, T. Björkman, P. Blaha, S. Blügel, V. Blum, et al., Reproducibility in density functional theory calculations of solids, Science 80 (2016) 351, https://doi.org/10.1126/science.aad3000.
[39] B.G. Johnson, M.J. Fisch, An implementation of analytic second derivatives of the gradient-corrected density functional energy, J. Chem. Phys. 100 (1994) 7429–7442, https://doi.org/10.1063/1.466887.
[40] J. Tang, A.C. Albrecht, Studies in Raman Intensity Theory, J. Chem. Phys. 49 (1968) 1144–1154, https://doi.org/10.1063/1.1670202.
[41] D.A. Long, The Raman Effect, John Wiley & Sons Ltd, Chichester, UK (2002), https://doi.org/10.1002/0470845767.
[42] J. Ferraro, Introductory Raman Spectroscopy, Elsevier (2003), https://doi.org/10.1016/B978-0-12-254105-6.X5000-8.
[43] C.A.A.S. Santos, R.J.C. Lima, P.F.F. Filho, A.O. dos Santos, J.A. Lima Jr, P.T.C. Freire, Low-wavenumber Raman spectra of L-tyrosine, L-tyrosine hydrochloride, and L-tyrosine hydrobromide crystals at high temperatures, J. Phys. Chem. Solids 136 (2020), https://doi.org/10.1016/j.jpcs.2019.109129 109129.
[44] U. von Barth, Basic Density-Functional Theory an Overview, Phys. Scr. T109 (2004) 9, https://doi.org/10.1238/Physica.Topical.109a00009.
[45] C. Zhao, H. Wu, A first-principles study on the interaction of biogas with noble metal (Rh, Pt, Pd) decorated nitrogen doped graphene as a gas sensor: A DFT study, Appl. Surf. Sci. 435 (2018) 1199–1212, https://doi.org/10.1016/j.apsusc.2017.11.146.
[46] P. Anandan, S. Vetrivel, R. Jayavel, C. Vedhi, G. Ravi, G. Bhagavannarayana, Crystal growth, structural and photoluminescence studies of L-tyrosine hydrobromide semi organic single crystal, J. Phys. Chem. Solids 73 (11) (2012) 1296–1301, https://doi.org/10.1016/j.jpcs.2012.06.015.
[47] H. Niu, X.Q. Chen, S. Wang, D. Li, W.L. Mao, Y. Li, Families of superhard crystalline carbon allotropes constructed via cold compression of graphite and nanotubes, Phys. Rev. Lett. 108 (2012), https://doi.org/10.1103/PhysRevLett.108.135501 135501.
[48] M. Ye, D. Vanderbilt, Ferroelectricity in corundum derivatives, Phys. Rev. B 93 (2016), https://doi.org/10.1103/PhysRevB.93.134303 134303.
[49] H. Sumiya, S. Satoh, High-pressure synthesis of high-purity diamond crystal, Diamond Rel. Mater. 5 (1996) 1359–1365, https://doi.org/10.1016/0925-9635(96)00559-6.